Uterus and cervix anatomical changes and cervix stiffness evolution throughout pregnancy

Erin M. Louwagie[1], Serena R. Russell[1], Jacqueline C. Hairston[2¤a], Claire Nottman[3]
Chia-Ling Nhan-Chang[2], Karin Fuchs[2], Cynthia Gyamfi-Bannerman[2¤b], Whitney
Booker[2], Maria Andrikopoulou[2], Alexander Friedman[2], Noelia Zork[2], Ronald Wapner[2],
Joy Vink[2¤c], Mirella Mourad[2], Helen M. Feltovich[4], Michael D. House[5], Kristin M.
Myers[1]*

1 Department of Mechanical Engineering, Columbia University, New York, NY, USA
2 Department of Obstetrics & Gynecology, Columbia University Irving Medical Center,
New York, NY, USA
3 Department of Biomedical Engineering, Columbia University, New York, NY, USA
4 Department of Obstetrics & Gynecology, Icahn School of Medicine at Mount Sinai,
New York, NY, USA
5 Department of Obstetrics & Gynecology, Tufts Medical Center, Boston, MA, USA

¤a Current Address: Department of Obstetrics & Gynecology, Northwestern Memorial
Hospital, Chicago, IL, USA
¤b Current Address: Department of Obstetrics, Gynecology & Reproductive Sciences,
University of California San Diego Health, La Jolla, CA, USA
¤c Current Address: Department of Obstetrics & Gynecology, Hawaii Pacific Health,
Honolulu, HI, USA
*kmm2233@cumc.columbia.edu

Abstract

The coordinated biomechanical performance, such as uterine stretch and cervical barrier
function, within maternal reproductive tissues facilitates healthy human pregnancy and
birth. Quantifying normal biomechanical function and detecting potentially detrimental
biomechanical dysfunction (e.g., cervical insufficiency, uterine overdistension, premature
rupture of membranes) is difficult, largely due to minimal data on the shape and size of
maternal anatomy and material properties of tissue across gestation. This study
quantitates key structural features of human pregnancy to fill this knowledge gap and
facilitate three-dimensional modeling for biomechanical pregnancy simulations to deeply
explore pregnancy and childbirth. These measurements include the longitudinal
assessment of uterine and cervical dimensions, fetal weight, and cervical stiffness in 47
low-risk pregnancies at four time points during gestation (late first, middle second, late
second, and middle third trimesters). The uterine and cervical size were measured via
2-dimensional ultrasound, and cervical stiffness was measured via cervical aspiration.
Trends in uterine and cervical measurements were assessed as time-course slopes across
pregnancy and between gestational time points, accounting for specific participants.
Patient-specific computational solid models of the uterus and cervix, generated from the
ultrasonic measurements, were used to estimate deformed uterocervical volume. Results
show that for this low-risk cohort, the uterus grows fastest in the inferior-superior
direction from the late first to middle second trimester and fastest in the
anterior-posterior and left-right direction between the middle and late second trimester.
Contemporaneously, the cervix softens and shortens. It softens fastest from the late first

to the middle second trimester and shortens fastest between the late second and middle third trimester. Alongside the fetal weight estimated from ultrasonic measurements, this work presents holistic maternal and fetal patient-specific biomechanical measurements across gestation.

Introduction

Pregnancy and parturition are remarkably mechanical processes, orchestrated by the growth, remodeling, and activity of maternal reproductive and gestational tissues. From the nonpregnant state to term gestation, the uterus, a thick-walled organ comprised predominantly of smooth muscle cells, sheathed in extracellular matrix (ECM), must remain quiescent as it grows in mass from about 70 to 1100 grams and stretches to accommodate intrauterine contents of around 10 milliliters in the nonpregnant state to 5 liters [1, 2]. As the uterus is stretched, the cervix, a collagen-rich organ connecting the intrauterine cavity to the vaginal canal, must remain closed to retain the fetus as it develops [3]. Similarly, the fetal membranes, a thin multi-layer tissue enclosing the fetus and amniotic fluid, must remain intact to provide mechanical support and protection from infection to the growing fetus [4]. At the time of parturition, these functions must all be reversed: the fetal membranes rupture, the cervix dilates, and the uterus contracts to allow for vaginal delivery. Though the exact mechanism(s) controlling these changes is unknown, it is clear that the mechanical failure and mistiming of these tissues can have catastrophic consequences.

In the prenatal period, one of the most common and dangerous outcomes is preterm birth (PTB, live birth before 37 weeks gestation). Globally, more than 1 in 10 babies is born preterm, and PTB-related complications are the leading cause of death for children under 5 years of age [5]. Cited causes of PTB with biomechanical implications are uterine overdistention, preterm premature rupture of membranes, and cervical insufficiency [6]. Still, the pathophysiology and interplay of these conditions remain unknown, and 70-80% of PTB is spontaneous and unexplained [6, 7]. The inability to accurately predict why and in whom PTB will occur has led to a lack of effective therapies for PTB prevention [8]. To truly understand how maternal reproductive anatomy supports the intrauterine load in uncomplicated pregnancies and target therapies in pregnancies at high risk for PTB, we must pursue computational approaches.

Pregnancy is a protected environment. Thus, *in-silico* approaches based on non-invasive measurements, such as ultrasound, are one of the only viable options for elucidating the biomechanical features of the pregnancy environment. Large institutional bodies have recognized the importance of computational modeling and simulation in clinical trials and device design, with the United States Food and Drug Administration (FDA) forming the Modeling and Simulation Working Group in 2016 and the American Society of Mechanical Engineers (ASME) releasing a standard for the verification and validation of computational models specifically for medical devices in 2018 [9, 10]. Advancements in *in-silico* methods for clinical study have facilitated vast research in fields such as cardiovascular, cartilage, and tumor growth biomechanics [11–13]. These methods can be used as digital twins to predict disease progression and tailor medical devices to individual patient needs. In pregnancy, these patient-specific models could include details such as previous cesarean section scars [14, 15]. The key roadblock in using computational methods to study and design devices for pregnancy complications, such as PTB, is a lack of data on biomechanical changes in human maternal reproductive tissues across gestation.

The first *in-vivo* data on maternal reproductive anatomy size and shape during pregnancy was published in 1950, where 15 pregnant uteri were imaged via x-ray at

regular intervals from 18 weeks of gestation until term, reporting outlines of the outer uterus and ratios of the inferior-superior to anterior-posterior uterine lengths [16]. However, x-ray imaging does not capture soft tissues well and is not commonly used in prenatal care today [16]. In 2010, ultrasound techniques were used to estimate uterine wall tension across gestation in 320 pregnancies (294 term singletons, 15 preterm singletons, and 11 twins), collecting measurements of inferior-superior, anterior-posterior, and left-right uterine diameter with anterior uterine wall thickness, though no cervical measurements were included [17]. The cervix is the most scrutinized of the maternal anatomic features during pregnancy, as cervical length can be used as a predictive tool for PTB, and time-course studies of cervical length and stiffness have been reported [18, 19]. In 2021, our team published the first datasets on uterine and cervical dimension measurements, cervical stiffness data, and computer-aided design (CAD) models of the uterus and cervix across gestation in 29 uncomplicated pregnancies, making all data and models publicly available to create wider opportunity for *in-silico* pregnancy research [20, 21].

In this study, we build upon previous work to quantify anatomical and biomechanical changes in the uterus and cervix across gestation in pregnant participants at low-risk for preterm birth. Our approach is to parametrically assess the size and shape of the uterus and cervix through a clinically implementable two-dimensional (2D) ultrasound protocol and measure *in-vivo* cervical stiffness via aspiration [20, 22]. Additionally, we use these parametric measurements to generate patient-specific CAD models across gestation. We present the following for pregnancies at low risk for PTB: 1) parametric dimension measurements of the uterus and cervix across gestation, 2) measurements of cervical stiffness via aspiration (Pregnolia AG, Schlieren, Switzerland), 3) the effects of gestational age on maternal reproductive anatomy with comparisons to previously published data [18, 20, 21], 4) patient-specific parametric CAD models of the uterus and cervix to estimate uterocervical tissue volume (Solidworks, Dassault Systémes, Vélizy-Villacoublay, France), and 5) corresponding measurements of fetal size and amniotic fluid level. This work makes available coordinated, patient-specific measurements of maternal reproductive tissue, the fetus, and cervical stiffness across gestation.

Methods

A prospective, time-course, observational study of human pregnancy in participants at low risk for PTB was conducted. Maternal reproductive anatomy, fetal size, and amniotic fluid level were measured via two-dimensional (2D) ultrasound and cervical stiffness using the Pregnolia system (Pregnolia AG, Schlieren, Switzerland). Measurements were collected at four time points during gestation: late first trimester (L1, 9w3d-15w3d), middle second trimester (M2, 17w3d-20w5d), late second trimester (L2, 23w3d-27w1d), and middle third trimester (M3, 33w4d-38w0d). Linear regressions were fit to the data to find relationships with gestational age, and T-tests were performed to analyze the effect of parity. All findings were compared to existing datasets on normal pregnancy.

Study Design

This was a prospective observational study of ultrasound dimension and cervical stiffness measurements in participants at low risk for PTB at 9w3d-15w3d, 17w3d-20w5d, 23w3d-27w1d, and 33w4d-38w0d gestation.

Participants

Participants were recruited from prenatal care patients at a single tertiary care center in New York, New York. Participants were approached after being introduced to the study by their primary obstetrician and consented to all study protocols prior to research participation. Fifty participants aged 23-41 were recruited and participated in the study from April 8, 2019 to June 17, 2023. Inclusion criteria included being 18 years of age or older, carrying an uncomplicated singleton gestation, and being able to provide informed consent. Exclusion criteria included a current IVF pregnancy, multifetal reduction, history of PTB, history of cervical surgery (LEEP, cone biopsy, trachelectomy, cerclage), history of cervical shortening in the current pregnancy, history of significant vaginal bleeding during pregnancy, history of any major abdominal/uterine surgery, history of cesarean section, abnormal pap smear, persistent cramping, persistent uterine contractions, vaginal bleeding at the time of consent, uterine anomalies, systemic or vaginal infections at the time of consent, on progesterone in the first trimester, fibroids, placenta previa or abnormal placentation, ovarian cysts (other than a corpus luteal cyst), and anything in vaginal canal in last 24 hours at the time of the first research visit. This study was approved by the institutional review board at Columbia University Irving Medical Center (CUIMC), and each participant provided written informed consent.

Participant age, height, weight, race, ethnicity, patient history, social history, and obstetric history were recorded for each patient. At each prenatal research visit, participants reported their weight, pregnancy complications since their last visit, and whether they'd had intercourse or other vaginal transition in the past 24 hours (tampon, yeast medication, etc.). After the participant delivered, the gestational age at delivery and mode of delivery (cesarean or vaginal) was recorded. Fifty participants were recruited to and participated in the study. Two participants delivered preterm (before 37 weeks gestation), and one miscarried. These participants were excluded from the analysis. Patient demographics for the remaining 47 participants are reported in table 1.

Table 1. Participant demographics and parity Number of subjects, N, and percentage of total subjects (in parentheses) in each group.

Demographic		N = 47	(%)
Age (years):	Mean ($\pm$ STD)	32 ($\pm$ 4)	
	Range	23-41	
Parity:	Nulliparous	30	(63.8)
	Multiparous	17	(36.2)
Ethnicity:	Hispanic	12	(25.5)
	Non-Hispanic	33	(70.2)
	Unknown/Not Reported	2	(4.3)
Race:	Asian	3	(6.4)
	Black/African American	6	(12.8)
	White	33	(70.2)
	Unknown/Not Reported	5	(10.6)

Ultrasound and Cervical Stiffness Measurements

Cervical stiffness was measured using the Pregnolia system (Pregnolia AG, Schlieren, Switzerland). This is an aspiration device administered during a speculum exam. Clinicians were trained to use the device following the "instructions for use" documentation and training videos provided by the Pregnolia website [23]. The system is operated via a control unit containing a vacuum pump attached to the probe by

flexible tubes. The vacuum is turned on via a foot pedal, creating a negative pressure at the probe head, and the clinician brings the probe head into contact with the distal anterior lip of the cervix. Once contact is established, the clinician slides the probe handle to the middle position, and the negative pressure is increased to pull the cervical tissue 4mm. The vacuum is stopped at this point, and the pressure required to displace the tissue 4mm is recorded. The measurement is performed three times. The average of these values is reported as the aspirated cervical stiffness (aCS).

Sonographers trained on the study protocol performed prenatal ultrasound examinations. Ultrasounds were collected by sonographers (I.K., I.M., and V.P.) trained on the ultrasound acquisition protocol by the material-fetal medicine specialist who initially developed it (C-L.N-C.). Before imaging, participants were asked to empty their bladders. Ultrasoound images were obtained using a GE Voluson E8 (GE Healthcare, Chicago, IL, USA). Standard clinical ultrasonic dimensions of the fetus were measured. Crown-rump length (CRL, cm) was measured at timepoint L1, and estimated fetal weight (EFW, grams) was measured at timepoints M2, L2, and M3. EFW was calculated using the Hadlock I formula, requiring measurements of biparietal diameter (BPD), head circumference (HC), abdominal circumference (AC), and femur length (FL) [24]. The maximum volume pocket (MVP, cm) was collected at all time points, and amniotic fluid index (AFI, cm) was collected at time points L2 and M3, and occasionally at M2. The placenta location was also recorded at all time points.

With the participant in the supine position, the three B-mode research images of maternal anatomy were acquired: transabdominal (TA) sagittal, TA axial, and transvaginal (TV) sagittal. The TA and TV images were collected following the protocol described in our previous work [20]. The TA images were acquired using extended field-of-view ultrasound imaging, where the probe was swept across the abdomen, and adjacent images were automatically registered to produce one long image. The extended field-of-view feature permitted imaging of the full length of the uterus in one image. The sonographer acquiring the images placed calipers on the images to mark the location of the dimension measurements at the time of image acquisition. Precise dimension measurements were later taken by E.M.L. using Fiji ImageJ [25]. Maternal-fetal medicine specialists M.H. and C-L.N-C reviewed images and measurements to verify adequate visualization of the structures under study, including notation of any problematic measurements, such as inaccurate cervical length resulting from a lower uterine segment contraction that distorts the anatomy.

From the TA sagittal ultrasonic image, the longest inferior-superior intrauterine diameter was measured from the fundal to the lower uterine segment endometrium (IS-UD), marking the inferior-superior intrauterine axis (Fig. 1a). Perpendicular to the midpoint of the inferior-superior intrauterine axis, the anterior-posterior intrauterine diameter (AP-UD) was measured (Fig. 1a). The TA axial ultrasonic image provided measurements of the longest left-right intrauterine diameter (LR-UD) (Fig. 1b). The TV sagittal image provided measurements of cervical length (CL), which was measured as the distance between the internal os (where the anterior and posterior cervix meet in the image) and the external os, and the smallest thickness of the lower uterine segment (LUS-UT) (fig. 1c). Additional ultrasonic measurements were collected to generate the patient-specific CAD models, but were not included in statistical analysis (S1 Appendix).

Estimated Uterocervical Volume

The estimated uterocervical volume (EUV) was found from solid models generated from the maternal ultrasonic dimensions. Parametric patient-specific CAD models were built in Solidworks 2018-19 (Dassault Systémes, Vélizy-Villacoublay, France) using an existing modeling protocol for all participant visits with ultrasonic dimension measurements (fig.

Fig 1. 2D ultrasonic measurements of the uterus and cervix. (A) Transabdominal panoramic 2D sagittal ultrasounds measured the inferior-superior (IS-UD) and anterior-posterior (AP-UD) intrauterine diameters. (B) Transabdominal panoramic 2D axial ultrasounds measured the left-right intrauterine diameter (LR-UD). (C) Transvaginal 2D sagittal ultrasounds measured cervical length (CL) and lower uterine segment thickness (LUS-UT). These dimensions are based on previously published measurement protocols [20, 26].

2 [20]. Several updates to the modeling protocol were made, as outlined in S1 Appendix. The EUV was found using the "Mass Properties" tool within Solidworks.

Fig 2. Uterus and cervix CAD models across gestation. Three-dimensional solid CAD models of the uterus and cervix for one participant from the late first to middle third trimester with the corresponding ultrasonic images. The top row is the isometric view, and the bottom is the sagittal view. The inferior-superior (IS-UD) and anterior-posterior (AP-UD) intrauterine diameters are marked in the sagittal view.

Statistical Analysis

A summary of participant numbers at each visit and those who attended the previous visit is provided in table S1 Table 1. Patient characteristics, uterine dimensions, cervical length, and cervical stiffness were analyzed in RStudio version 1.3.1056 [27]. Ultrasound measurements and cervical stiffness were analyzed using a linear regression accounting for differences in both parity and participant. Welch's t-tests were used to determine measurement differences between cohorts and visits. For the slope comparisons, the hypothesis is that there is no difference between the measurements from the two time points being assessed. The assessed slopes are overall (L1-M3) and between visits (L1-M2, M2-L2, L2-M3). P-values under 0.05 are considered significant and denoted by a star. Means, standard deviations, and regression coefficients were calculated in R. All graphs were created in R. All code used in the statistical analysis is available through Columbia University Library's Academic Commons (URL: provided upon paper acceptance).

Results

All maternal and fetal ultrasonic measurements, patient-specific CAD models of reproductive anatomy, and estimated combined uterus and cervix volume data are available through Columbia University Library's Academic Commons (URL: provided upon paper acceptance).

Maternal ultrasonic measurements

Ultrasonic measurements of maternal anatomy varied across participants, and gestational age impacted each analyzed ultrasonic measurement of maternal anatomy differently. All uterine diameters increased across gestation (fig. 3). Overall, IS-UD increased by 8.2 mm/week, AP-UD by 2.1 mm/week, and LR-UD by 6.3 mm/week (tab. 2). The periods of greatest increase differed between intrauterine diameters, with the largest slope for IS-UD between L1-M2 (10.5 mm/week) and the largest slope for AP-UD and LR-UD between M2-L2 (2.4 and 8.7 mm/week, respectively). LUS-UT and CL decreased as gestational age increased. LUS-UT significantly decreased across gestation (tab. 2), with the most significant thinning between L2-M3

Table 2. Mean dimension measurements and slopes. Mean and standard deviation (STD) for 2D ultrasonic and cervical stiffness measurements across all participants and gestation ages. Overall (L1-M3) and between visit slopes for 2D ultrasonic measurements with participant correlation. Asterisks indicate significance level: $P < .05$ ( ), $P = .01\text{-}.05$ (*), $P = .001\text{-}.01$(**), $P < .001$ (***).

| | Mean±STD (mm) | | | | Slope (mm/week) | | | |
	L1	M2	L2	M3	Overall	L1-M2	M2-L2	L2-M3
IS-UD	81.7±17.8	151.5±16.3	201.8±21.6	269.5±28.3	8.2***	10.5***	7.9***	6.3***
AP-UD	49.3±14.2	61.5±9.5	73.8±11.7	98.3±23.1	2.1***	1.7***	2.4***	2.3***
LR-UD	85.8±12.2	131.6±16.7	184.3±21.3	224.8±21.6	6.3***	6.7***	8.7***	4.1***
LUS-UT	5.0±1.5	4.9±2.0	4.7±1.8	3.6±1.3	-0.1***	-0.1	0.0	-0.1**
CL	41.7±5.7	41.4±5.3	42.0±4.8	37.1±6.4	-0.2***	0.0	-0.1	-0.5***
aCS (mbar)	128±51	91±36	74±39	61±30	-3***	-5***	-2	-1

Fig 3. Intrauterine diameters with gestational age. (A) Inferior-superior (IS-UD), (B) anterior-posterior (AP-UD), and (C) left-right (LR-UD) intrauterine diameter with gestational age for all participants. The dotted line marks the overall slope, and participants are color-coded by parity (blue = nulliparous, orange = multiparous).

(-0.1 mm/week). The slope of CL decrease (fig. 4) was -0.2 mm/week (tab. 2), with the greatest and only significant decrease in L2-M3 (-0.5 cm/week). No parity-based significant differences in means or slopes were found for any maternal measurements included in the analysis (S2 Table 1). Of note, transvaginal images taken during a lower uterine segment contraction (n=18) were not included in the slope analysis.

Fig 4. LUS-UT, CL, and aCS with gestational age. (A) Lower uterine segment thickness (LUS-UT), (B) cervical length (CL), and (C) aspirated cervical stiffness (aCS) with gestational age for all participants. The dotted line marks the overall slope, and participants are color-coded by parity (blue = nulliparous, orange = multiparous).

Aspirated cervical stiffness measurements

The aspirated cervical stiffness (aCS) values found across participants throughout gestation fell within previously reported values for pregnancies at low-risk for PTB (fig. 4), with ranges similar to that reported in Badir et al. [18]. Across gestation, cervical stiffness decreased with increasing gestational age by -3 mbar/week (tab. 2). The only significant change in cervical stiffness between visits was L1-M2 (-5 mbar/week). This was also the largest decrease between visits. No significant differences were found in aCS value means or slopes based on parity (S2 Table 1).

Estimated uterocervical volume and fetal weight

The estimated uterocervical volume (EUV) and fetal weight (EFW) increased for all participants across gestation (fig. 5).

Fig 5. Estimated uterocervical volume (EUV) and fetal weight (EFW) across gestation. Mean estimated uterocervical volume ([mm^3], solid blue line) and estimated fetal weight ([g], dashed black line) across gestation with standard deviation (gray).

Discussion   225

This novel clinical dataset of human pregnancy presents time-course measurements of   226
maternal uterocervical geometry, cervical stiffness, and fetal size. Participants attended   227
four research visits from the late first to the middle third trimesters during which 2D   228
ultrasound images were acquired of the uterus, cervix, and fetus. We found that   229
intrauterine diameters increase with gestational age, with the rate of increase dependent   230
on gestational age, which is logical since the uterus must grow and stretch to   231
accommodate the growing fetus and increasing amniotic fluid volume. The largest   232
increase was found in IS-UD, the smallest in AP-UD, and LR-UD fell in between. These   233
findings suggest less mechanical resistance to uterine growth superior, as compared to   234
inferior, to the uterus. This makes sense, since since the uterus is bound inferiorly by   235
the bony pelvis while the space superior to it contains primarily soft internal organs.   236
The mechanical rationale for why LR-UD increases more than the anterior-posterior   237
intrauterine diameter warrants further exploration. We hypothesize this is because the   238
AP boundaries (anterior = abdominal well, posterior = spine) are more restrictive than   239
the lateral boundaries. In a previous study of maternal anatomy in which we   240
investigated uterine diameters in the standing and supine positions, we found   241
gravity-based differences in AP-UD trends. For example, the AP-UD overall, AP-UD   242
late first to early second-trimester, and LR-UD late second to middle third slopes were   243
significantly larger in the standing compared to the supine position (S2 Table 2) [20].   244
This has implications for future digital twin studies in which maternal position is   245
considered. However, the AP-UD slope was smaller for all gestational time points than   246
the LR-UD slope. Lastly, we found a positive relationship between all intrauterine   247
diameters and EFW, allowing for the estimation of IS-UD, AP-UD, and LR-UD from   248
EFW in scenarios where extended-field-of-view imaging is not available, and exact   249
intrauterine diameter values are not necessary (fig. 6).   250

Fig 6. Intrauterine diameters graphed with estimated fetal weight. (A)
Inferior-superior (IS-UD), (B) anterior-posterior (AP-UD), and (C) left-right (LR-UD)
intrauterine diameters with corresponding estimated fetal weight (EFW). A linear
regression was fit for each, with R^2 values between $0.69 - 0.79$ for all. Individuals were
plotted according to parity (orange = nulliparous, blue = multiparous).

Features of cervical remodeling palpable to the clinician include decreasing cervical   251
stiffness and length. Unsurprisingly, we found that aCS decreased with CL and LUS-UT.   252
For example, the LUS-UT decrease was statistically significant across gestation and   253
between the late second and middle third trimesters (tab. 2). The aCS and CL   254
decreased significantly across gestation, though not at the same rate. The cervix softens   255
the most between the late first and middle second trimester, whereas the cervix   256
shortens the most between the late second and early third trimester (tab. 2). This trend   257
of cervical softening before shortening has been reported in previous cervical aspiration   258
studies in humans [18, 28]. Numerous studies in rodents and macaques support this   259
finding and provide insight into the underlying tissue changes [29, 30]. Specifically,   260
though the collagen content (per dry weight) in the cervix remains constant during   261
pregnancy, its hierarchical structure remodels drastically through constant synthesis,   262
assembly, and degradation of collagen fiber components [30–32]; in the nonpregnant   263
cervix, collagen fibers are highly organized and cross-linked. As pregnancy progresses,   264
collagen crosslink maturity declines the most in mid-pregnancy, corresponding to the   265
fastest decline in tissue stiffness [30, 32]. Our work demonstrating the dynamic profile of   266
cervical length and stiffness changes suggests that, while the cervix softens early in   267
pregnancy, the mechanical load from the uterine wall's pull and the amniotic sac's push   268
is not large enough to deform it until the late second trimester when the LUS thin and   269

cervix shortens at its fastest rate as fetal growth accelerations (fig. 5).   270

Comparisons to previously published data   271

A detailed comparison between the data presented and an existing longitudinal cohort   272
study is presented in S2 Appendix [20]. Both cohorts demonstrate a significant   273
difference in overall LUS-UT slope, with the existing cohort exhibiting a statistically   274
significant decrease between each research visit [20]. However, no significant differences   275
for between visit slopes are found between cohorts, further supporting our finding that   276
LUS-UT thins most beginning the late second trimester (tab. S2 Table 3).   277

Several other existing studies involving measurements of lower uterine segment wall   278
thickness across gestation agree with our findings. Degani et al. reported a significant   279
decrease in LUS thickness in 25 uncomplicated pregnancies at 8-week intervals between   280
15-39 weeks gestation [33]. Similarly, Ginsberg et al. found the lower uterine segment to   281
thin with increasing gestational age in a cross-sectional study of 350 singleton   282
uncomplicated pregnancies from 15 to 42 weeks gestation [34]. Neither of these studies   283
analyzed rate of thinning [33, 34]. Durnwald et al. evaluated LUS in a cross-sectional   284
study of 175 singleton uncomplicated pregnancies in the first, second, and third   285
trimesters [35]. Dissimilar to our findings, they reported significant lower uterine   286
segment wall thinning between the first and second, but not between the second and   287
third, trimester [35]. A key methodological difference between Durnwald et al. and us is   288
performance of the LUS measurement 2cm above the internal os in a TA image with a   289
full bladder, whereas we measured the thinnest segment of the anterior uterine wall in a   290
TV image with an empty bladder [35].   291

Many previous studies show that the cervix softens during pregnancy. Using the   292
same linear regression approach on an existing dataset of shear wave speed across   293
pregnancy by Carlson et al., the overall slope decreased across gestation, with the   294
largest decrease occurring between the late first and early second trimesters, concuring   295
with the aCS slopes presented here (S2 Table 3) [21]. Carlson et al. also found that the   296
greatest decrease in shear wave speed occurred closest to the proximal cervix, with a   297
significant non-linear trend, and no significant trends in the distal cervix [21].   298
Longitudinal elastography studies have shown softening throughout   299
pregnancy [19, 36–40], though no others noted significant early softening. It seems   300
important to establish a normal rate of softening, especially early in pregnancy, because   301
premature and/or accelerated softening is logically associated with risk of PTB. For   302
example, a cervical aspiration study demonstrated that patients presenting for cerclage   303
due to a history of preterm birth and short cervical length have significantly softer   304
cervices than normal controls [28]. Another demonstration of softening early in normal   305
pregnancy is provided by Badir et al. in a study of 100 patients at low risk for PTB [18].   306
Importantly, the aCS mean and standard deviation reported in that study overlat with   307
that of ours (S2 Fig. 1). In summary, the agreement across studies of progression in   308
cervical softening is promising and warrants further material modeling efforts to   309
determine relationships in cervical stiffness changes measured via different modalities.   310

Limitations   311

Though this work presents a novel dataset of maternal and fetal growth with changes to   312
cervical stiffness across pregnancy, it has limitations. Our participants were   313
predominantly white, thus study of more diverse populations is imperative. Further, the   314
dataset is incomplete, with missed participant visits due to scheduling conflicts,   315
inclement weather, participant dropouts due to changing providers, the coronavirus   316
pandemic, and being lost to follow-up. Scheduling conflicts also led to lack of cervical   317
aspiration measurements at some research visits due to unavailability of trained   318

physicians. Further, while the aCS differences were observed in some patients across the three average measurements, with ranges greater than 50 mbar for 16 L1 measurements, 3 M2 measurements, 1 L2 measurement, and 1 M3 measurement are likely due to the viscoelastic behavior of the cervix, it is possible that other factors could contribute to these measurement ranges. These include cervical surface friction, force applied to the probe during measurement, and differences in inter-operator technique, all of which deserve focused evaluation in future studies. Ultrasonic measurements may be compromised by inter-operator variability [20], though we attempted to minimize this by having an experience clinician verify all dimensions. In some of the research visits, the clinician deemed dimensions "unmeasurable" due to poor visualization and/or acquisition. While this reflects the "real world" situation, these measurements were excluded from statistical analysis, though estimates were used to generate the solid models for the estimated uterocervical volume and are included in the available dataset (data sets published by Columbia Academic commons; URL provided up acceptance). Finally, measurements of estimated uterocervical volume have not been verified for gestational ages of less than 37 weeks, and thus it is unknown how errors in ultrasonic measurements may propagate to errors in estimated uterocervical volume.

Conclusion

This work presents holistic measurements of changes to maternal anatomy with progressive growth of the reproductive structures and fetus during pregnancy on a patient-specific basis, with complementary measurements of cervical softening. Anatomic measurements of the uterus, cervix, and fetus were collected using typical clinical B-mode 2D ultrasound acquisitions. The uterine diameter increased most in the inferior-superior direction and least in the anterior-posterior direction. The lower uterine segment thinned significantly across gestation as the cervical stiffness and length decreased. The most rapid cervical softening occurred between the late first and middle second trimester, whereas the greatest shortening occurred between the late second and middle third trimester. These findings quantitatively characterize changes in the uterus and cervix in normal pregnancy, providing a foundation for *in-silico* studies of digital twins that can be manipulated to model multiple pregnancy situations.

Supporting information

S1 Appendix.   Supplemental Methods In addition to the methods outlined in this work, the authors provide further details on the available data, Columbia University (CU) and Intermountain Healthcare (IH) cohorts, and estimation of uterocervical volume from patient-specific computer-aided design models (digital twins). The IH cohort was originally published in [20].

Not all participants in the Columbia University cohort could make it to all four research visits, and not all research visits could include cervical stiffness measurement. A summary of how many participants attended each research visit timeframe and the number of ultrasonic and aspiration measurements collected is presented in S1 Table 1. The number who attended the prior visit is also given, which is pertinent for the between-visit analysis.

S1 Table 1   Research visit attendance. Summary of the number of participants who attended during each visit timeframe and the number who attended the previous visit.

	L1 (9^3-15^3)	M2 (17^3-20^5)	L2 (23^3-27^1)	M3 (33^4-38^0)
Attended visit	45	37	34	29
Ultrasound collected	45	37	33	28
Aspiration collected	43	35	29	24
Attended prior visit	N/A	35	32	28

Though the between-visit slope in the CU and IH cohorts were directly compared, the gestational age range for each visit did not exactly overlap. In the case of visit 2, there is no overlap in gestational age between the two cohorts. The gestational age range and number of participants for each visit in the CU and IH cohorts are given in S1 Table 2.

S1 Table 2   Visit timeframes for Columbia University (CU) and Intermountain Healthcare (IH) cohorts. Some overlap in gestational age exists for all research visits, with the exception of visit 2.

	Visit 1	Visit 2	Visit 3	Visit 4
CU Gestational Age	L1 (9^3-15^3)	M2 (17^3-20^5)	L2 (23^3-27^1)	M3 (33^4-38^0)
CU participants	45	37	34	28
IH Gestational Age	L1 (8^3-14^5)	E2 (15^3-16^6)	L2 (22^0-24^6)	M3 (32^0-34^4)
IH participants	29	29	29	29

The set of maternal anatomic dimensions on which linear regressions were performed was analyzed because they previously demonstrated excellent agreement between observers, except cervical length (good agreement), and represent gross uterine and cervical size. However, they do not characterize the shape of the uterus and cervix, which is necessary to generate parametric patient-specific computer-aided design (CAD) models. Here, we list all maternal anatomic dimensions collected and made available through Columbia University's Academic Commons (URL provided up acceptance). These dimensions are based on previous definitions, and all measured dimensions were checked by a maternal-fetal medicine clinician (M.H.) [20, 26]. For clarity, the set of measurements on which linear regressions were performed were referred to using anatomic descriptors, i.e. inferior-superior intrauterine diameter is IS-UD. Previous work did not use this naming approach, so we present the anatomic descriptors in bold next to the equivalent dimensions.

From the transabdominal sagittal ultrasonic image, the following dimensions were measured:

- UD1 (**IS-UD**): longest inferior-superior intrauterine diameter was measured from the fundal to the lower uterine segment endometrium (S1 Fig. 1a)

- UD2: anterior intrauterine diameter, measured perpendicularly from midpoint of UD1 to anterior intrauterine wall (S1 Fig. 1a)

- UD3: posterior intrauterine diameter, measured perpendicularly from midpoint of UD1 to posterior intrauterine wall (S1 Fig. 1a)

- UD23 (**AP-UD**): sum of UD2 and UD3 (S1 Fig. 1a)

- UT1: fundal uterine wall thickness, measured as close to the superior end of UD1 as possible (S1 Fig. 1a)

- UT2: anterior uterine wall thickness, measured at the anterior end of UD2 (S1 Fig. 1a)

- PCO: perpendicular cervical offset, perpendicular distance between UD1 and internal os (S1 Fig. 1a)

- UD3a_eq: posterior dimension perpendicular to UD1 at 25% of UD1 from the superior intrauterine wall (S1 Fig. 1a)

- UD3b_eq: posterior dimension perpendicular to UD1 at 75% of UD1 from the superior intrauterine wall (S1 Fig. 1a)

- UD3a_ex: extrema perpendicular distance between posterior wall and UD1 superior to UD3, no always applicable (S1 Fig. 1b)

- UD1a_ex: distance from inferior end of UD1 to UD3a_ex, only measured if UD3a_ex was measured (S1 Fig. 1b)

- UD3b_ex: extrema perpendicular distance between posterior wall and UD1 inferior to UD3, no always applicable (S1 Fig. 1b)

- UD1a_ex: distance from inferior end of UD1 to UD3b_ex, only measured if UD3b_ex was measured (S1 Fig. 1b)

S1 Fig. 1   Solid Modeling Measurements. (A) Measurements collected from sagittal ultrasound images to capture the sagittal uterine shape and placement of the cervix, with measurements of posterior intrauterine diameter taken equidistantly (eq) along UD1. (B) Alternative method to collecting posterior intrauterine diameter measurements, taken at the superior (UD3a) and inferior (UD3b) extrema (ex). (C) Measurements collected from axial ultrasound images to capture the axial uterine shape. (D) Measurements taken from sagittal transvaginal ultrasounds to capture the uterus and cervix. (E) Measurements of outer cervical diameter taken equidistantly along the cervical length. (F) Measurements of inner cervical diameter taken equidistantly along the cervical length.

From the TA axial ultrasonic image, the following dimensions were measured:

- UD4 (**LR-UD**): longest left-right intrauterine diameter (S1 Fig. 1c)

- UT3: left/right uterine wall thickness, measured as close to the left or right end of UD4 as possible (S1 Fig. 1c)

From the TV sagittal image, the following dimensions were measured:

- UT4 (**LUS-UT**): lower uterine segment thickness, measured as the thinnest portion of the visible anterior uterine wall (S1 Fig. 1d)

- **CL**: cervical length, measured as the distance between the internal os (where the anterior and posterior cervix meet in the image) and the external os (S1 Fig. 1d)

- AUCA: anterior uterocervical angle, measured as the angle between the lower uterine segment and cervical canal, placed as 1 cm lines starting at the internal os along the anterior uterine wall and the cervical canal (S1 Fig. 1d)

- CD1_25: outer cervical diameter measured at 25% of CL from the internal os (S1 Fig. 1e)

- CD1_50: outer cervical diameter measured at 50% of CL from the internal os (S1 Fig. 1e)

- CD1_75: outer cervical diameter measured at 75% of CL from the internal os (S1 Fig. 1e)

- CD2_25: inner cervical diameter measured at 25% of CL from the internal os (S1 Fig. 1f)

- CD2_50: inner cervical diameter measured at 50% of CL from the internal os (S1 Fig. 1f)

- CD2_75: inner cervical diameter measured at 75% of CL from the internal os (S1 Fig. 1f)

Of these maternal anatomic dimensions, the only ones not used in the parametric patient-specific models are CD1_25, CD1_75, CD2_25, and CD2_75. Future iterations of the modeling approach may include them to attain a more refined cervical shape.

The approach to modeling the uterus was updated slightly from the previous method [20]. First, due to the variability in sagittal posterior uterine wall shape observed between patients and gestational ages, several methods of building the posterior wall were generated based on parametric measurements collected (updating fig.5a in [20]). If both the superior (UD3a) and inferior (UD3b) posterior diameter measurements were collected as extremum (ex), quarter ellipses were used at the inferior and superior ends of the uterus with a spline connecting them through the middle posterior diameter (UD3) (S1 Fig. 2a). A spline was used for the entire posterior uterine profile if no posterior diameters were measured as extremum, thus using the equidistant (eq) approach (S1 Fig. 2b). Finally, if only one of the inferior (S1 Fig. 2c) or superior (S1 Fig. 2d) posterior diameter measurements were collected as extremum, a quarter ellipse was used at the end with the extremum measured, and a spline connecting the middle posterior diameter and equally placed measurement of posterior diameter to the end of the inferior-superior axis.

S1 Fig. 2   Sagittal uterine modeling approaches. Method to model the sagittal uterus when (A) both superior (UD3a_ex) and inferior (UD3b_ex) posterior intrauterine diameters are taken as extrema, (B) both superior (UD3a_eq) and inferior (UD3b_b) are taken equidistantly along the inferior-superior axis, (C) only the inferior (UD3b_ex) is taken as extrema, and (D) only the superior (UD3a_ex) is taken as extrema. Red arrows depict the ends of the spline, where tangency constraints are enforced.

The method of generating the uterine body was also updated, with an inferior-superior loft through axial profiles used rather than a left-right loft function, updating fig.5c in [20]. The coronal uterine shape was still modeled as an ellipse, with elliptical profiles placed coincidentally with UD3a and UD3b (**??**a). The intrauterine diameters at these locations were assigned by their location within the coronal ellipse defined by UD1 and UD4, with UD4a given by eq. 1 and UD4b given by eq. 2.

$$UD4a = 2 * (UD4/UD1) * \sqrt{UD1a} * (UD1 - UD1a) \tag{1}$$

$$UD4b = 2 * (UD4/UD1) * \sqrt{UD1b} * (UD1 - UD1b) \tag{2}$$

For the outer uterus, eq. 1 and eq. 2 were modified such that the superior and inferior uterus were defined to include uterine wall thicknesses (UT1 and UT4, respectively).

The anterior-posterior diameter of the axial elliptical profiles was defined by the sagittal uterine profile (**??**b), and the loft function executed using the sagittal profile as guides (**??**c).

S1 Fig. 3 Uterine body modeling approach. The uterine body modeling approach was updated to enforce an elliptical axial cross section. (A) Left-right diameters were placed coincidentally at locations with a posterior intrauterine diameter to generate an elliptical coronal cross section. (B) Axial ellipses are generated at each location with a posterior intrauterine diameter to be defined by the left-right intrauterine diameters and sagittal uterine profile. (C) The uterine body is generated using the loft functions, with the sagittal shape acting as guides and the axial ellipses acting as loft profiles.

S2 Appendix.   Additional Analyses In addition to the analyses on changes in intrauterine diameter, lower uterine segment thickness, and cervical length with gestational age, analyses on the effects of parity and maternal position were performed. Comparison between cohorts and to existing datasets was also undertaken to assess our findings.

All measurements of fetal anatomy and amniotic fluid levels were compared to clinically established growth charts (data sets published by Columbia Academic commons; URL provided up acceptance), and few anomalies were identified. Crown-rump length measurements were compared against the INTERGROWTH-21st Project's crown-rump length percentiles during the first trimester, with 40 out of 43 measurements within the 5th-95th percentile [41]. Similarly, 95 out of 101 measurements of estimated fetal weight were within the 5th-95th percentile based on data from the World Health Organization [42]. Finally, 93 out of 100 maximum vertical pocket measurements and 52 out of 57 amniotic fluid index measurements were within the 5th-95th percentile based on data from the National Institute of Child Health and Development [43]. Thus, the pregnancies analyzed in the study are, for the most part, within normal ranges.

In analyzing parity in the Columbia University (CU) cohort, presented in this study, no significant difference was found in mean for any of the analyzed measurements at any gestational age between nulliparous and multiparous participants (S2 Table 1). This aligns with previous work, which reports no significant difference in lower uterine segment thickness based on parity [33,34]. However, it is contradictory to the findings of Durnwald et al., who reported a significant difference between nulliparous and multiparous lower uterine segment thicknesses, though these results appear to include measurements from all three trimesters [35].

S2 Table 1 Effect of parity on maternal ultrasonic measurements. Mean ± standard deviation for nulliparous and multiparous participants during the late first (L1), middle second (M2), late second (L2), and middle third (M3) trimester with the corresponding Welch's T-test p-value. Performed for inferior-superior (IS-UD), anterior-posterior (AP-UD), and left-right (LR-UD) intrauterine diameters and lower uterine segment thickness (LUS-UT), cervical length (CL), and aspirated cervical stiffness (aCS).

Given the difference between visit slopes found in the CU cohort, the same analysis was undertaken in the Intermountain Healthcare (IH) cohort to compare slopes in the standing and supine position (S2 Table 2). Previously, it was reported that position significantly affected slopes for all intrauterine diameters, but not lower uterine segment

	IS-UD	AP-UD	LR-UD	LUS-UT	CL	aCS
L1 Mean ± STD (mm)						
Multiparous	83.6±15.7	45.2±14.6	88.9±10.8	7.8±4.0	47.5±11.4	131±34
Nulliparous	80.6±19.1	50.1±14.1	83.9±12.8	7.5±7.2	47.4±8.8	127±61
Parity T-test	0.56	0.27	0.17	0.88	0.99	0.77
E2 Mean ± STD (mm)						
Multiparous	151.4±16.4	65.1±8.6	129.2±18.2	5.8±3.0	44.8±11.1	87±40
Nulliparous	151.5±16.6	59.5±9.6	132.9±16.1	6.4±4.6	44.5±5.7	94±34
Parity T-test	0.98	0.08	0.54	0.61	0.91	0.58
L2 Mean ± STD (mm)						
Multiparous	208.0±19.3	70.5±9.9	187.1±17.4	5.8±2.7	42.4±7.3	59±29
Nulliparous	198.6±22.4	75.8±12.4	182.8±23.2	5.2±4.2	45.1±6.8	83±41
Parity T-test	0.23	0.19	0.56	0.58	0.31	0.08
M3 Mean ± STD (mm)						
Multiparous	275.8±24.7	103.6±12.9	232.8±21.9	3.9±1.4	36.0±7.0	61±32
Nulliparous	264.7±30.6	100.5±14.3	218.9±20.1	3.4±1.1	38.7±6.5	60±28
Parity T-test	0.30	0.55	0.10	0.27	0.32	0.98

thickness or cervical length [20]. The patient-correlated linear regression analysis
approach found no significant difference in the inferior-superior intrauterine diameter
(IS-UD) overall or between any visits. This approach found a significant difference in
the overall slope of anterior-posterior intrauterine diameter (AP-UD) and L1-E2 slope,
with the supine slope being smaller than the standing slope in both cases. The only
significant difference found in left-right intrauterine diameter slope (LR-UD) was found
between L2-M3, with the supine slope being smaller than the standing slope. No
significant difference was found in lower uterine segment thickness (LUS-UT) and
combined cervical and isthmus length (CL+IS) for any slope between standing and
supine.

S2 Table 2   Effect of position on overall and between visit slope. Overall and
between visit slopes for Intermountain Healthcare (IH) cohort 2D ultrasonic
measurements with participant correlation in the standing and supine position with
Welch's T-test p-value. Visit occurred in the late first (L1), early second (E2), late
second (L2), and middle third (M3) trimesters. Asterisks indicate significance level
compared to the null hypothesis (slope is zero): $P <.05$ ( ), $P = .01-.05$ (*), $P = .001-.01$ (**), $P <.001$ (***).

	Overall Slope (mm/week)			L1-E2 Slope (mm/week)			E2-L2 Slope (mm/week)			L2-M3 Slope (mm/week)		
	Supine	Standing	p-val	Supine	Standing	p-val	Supine	Standing	p-val	Supine	Standing	p-val
IS-UD	8.7***	9.0***	0.82	7.9***	7.8***	0.26	9.1***	9.2***	0.73	8.8***	9.4***	0.25
AP-UD	2.6***	3.0***	<0.001	2.1***	4.3***	<0.001	2.6***	2.2***	0.39	2.7***	2.9***	0.56
LR-UD	7.6***	8.2***	0.57	5.8***	5.5***	0.74	9.5***	8.4***	0.21	6.8***	9.2***	0.008
LUS-UT	-0.32***	-0.35***	0.94	-0.7*	-0.5	0.65	-0.5*	-0.5*	0.78	-0.2*	-0.2*	0.46
CL+IS	-0.5***	-0.6***	0.87	0.1	-0.3	0.74	-0.5	-0.6	0.85	-0.9**	-0.9**	0.95

The changes in maternal ultrasonic measurements were compared to the existing
serial dataset collected at Intermountain Healthcare (IH) in Provo, Utah [20]. Similar to
this study, patients at low risk for PTB underwent the same ultrasonic scanning
protocol in the late first, early second, late second, and middle third trimesters, with
images collected with participants in both the standing and supine position. Cervical
stiffness was measured at each visit via ultrasonic shear wave speed (SWS) [21]. The

original analysis of these data presented linear mixed effects models for each ultrasonic parameter to estimate its relationship with gestational age, position, and parity [20]. To directly compare the presented dataset (CU) and previous dataset (IH), the same patient-correlated linear regression analysis was performed, and a Welch's t-test was done to find significant differences (tab. S2 Table 3). Cervical length was combined with isthmus length (CL+IS) in the IH cohort to match the CU study protocol. Also, all CU cervical and lower uterine segment measurements were included for comparison, as the presence of contraction in TV images is considered a subjective finding and methods for identification may not be the same between cohorts [44].

In Carlson et al., shear wave speed (SWS) measurements were collected at 5 gestational ages to measure changes in cervical stiffness [21]. The first four visits coincide with those from Louwagie et al., thus the fifth visit was not included in this analysis [20]. At each visit, three SWS images were taken, and split into 4 regions in the anterior cervix: proximal (P), mid-proximal 1 (MP1), mid-proximal 2 (MP2), and middle (M) [21]. All SWS data is publicly available, and each image produces 100-200 SWS values in each of the four cervical regions. To determine a shear wave speed measurement for each participant at each visit, all P, MP1, MP2, and M measurements were averaged across all values from all 3 SWS images. To quantify the relationship between gestational age and SWS, 4 linear regressions were performed to find the overall slope and slope between visits 1-2, 2-3, and 3-4. The data averaging and the linear regressions were both performed in RStudio version 2023.6.0.421 [27].

S2 Table 3 Comparison between Columbia University (CU) and Intermountain Healthcare (IH) cohorts [20]. Overall and between visit slopes for IH cohort in supine position, with Welch's t-test P-values against CU cohort (P-value).

	Overall (mm/week)		L1-E2 (mm/week)		E2-L2 (mm/week)		L2-M3 (mm/week)	
	IH Slope	P-value	IH Slope	P-value	IH Slope	P-value	IH Slope	P-value
IS-UD	8.7***	0.75	7.9***	0.03	9.1***	0.79	8.8***	0.18
AP-UD	2.6***	<.001	2.1***	0.67	2.6***	0.15	2.7***	0.62
LR-UD	7.6***	0.89	5.8***	0.29	9.5***	0.31	6.8***	<.001
LUS-UT	-0.3***	<.001	-0.7*	0.58	-0.5*	0.23	-0.2*	0.67
CL+IS	-0.5***	0.24	0.11	0.03	-0.5	0.57	-0.9**	0.31
SWS (m/s)	-0.07***	N/A	-0.13	N/A	-0.10*	N/A	-0.05*	N/A

Overall slopes were significantly different for AP-UD and LUS-UT, though the qualitative findings remain the same: AP-UD increases across gestation, and LUS-UT decreases (S2 Table 3). Additional differences are observed in the timeframe of the greatest increase in intrauterine diameters, with IS-UD increasing most between E2-L2, AP-UD increasing most from L2-M3, and LR-UD increasing most from E2-L2. That said, significant differences were only found for IS-UD between L1-E2 timeframe and LR-UD between L2-M3. A notable difference is also observed in LUS-UT slopes across gestational age, with significant decreases observed between each research visit, the largest of which occurs between L1-E2. However, no significant difference between the CU and IH datasets for LUS-UT between visit slopes was found.

CL significantly decreased between L2-M3 in the IH cohort, with no significant difference to the CU cohort. Differences in LUS-UT definition may also contribute to the inconsistencies between datasets, where LUS-UT was specifically measured in the thinnest portion of the lower uterine segment in the CU cohort but not in the IH cohort. Cervical stiffness was also collected in the IH cohort, but since SWS was measured and not aspiration, no direct quantitative comparisons can be made without a non-linear, time-dependent material model. However, the overall SWS slope decreased across

gestation, with the largest (though insignificant) decrease occurring between L1-E2, which concur with the CU cohort's aCS slopes (S2 Table 3).

Changes in cervical stiffness with gestation found in the CU cohort were compared to previous findings in aspirated cervical stiffness (aCS) and shear wave speed (SWS) [18, 21]. No raw data was publicly available for aCS with gestational age, so the published figure on mean aCS values with gestational age was reproduced with the CU cohort overlaid (S2 Fig. 1). Plotting the aCS data as such, there appears to be good overlap between the two datasets, with the means of both falling within one standard deviation of the closest gestational age.

S2 Fig. 1 Aspirated cervical stiffness for CU cohort and Badir et al. 2013. Mean and standard deviation of aspirated stiffness value across gestation in the Columbia University (CU) cohort and data from Badir et al. [18].

Acknowledgments

References

1. Myers KM, Elad D. Biomechanics of the human uterus. WIREs Systems Biology and Medicine. 2017;9(5):e1388. doi:10.1002/wsbm.1388.

2. Cunningham FG, Leveno KJ, Bloom SL, Dashe JS, Hoffman BL, Casey BM, et al. Maternal Physiology. In: Williams Obstetrics, 25e. New York, NY: McGraw-Hill Education; 2018.Available from: obgyn.mhmedical.com/content.aspx?aid=1160772082.

3. Yoshida K. Bioengineering and the cervix: The past, current, and future for addressing preterm birth. Current Research in Physiology. 2023;6:100107. doi:10.1016/j.crphys.2023.100107.

4. Menon R, Lappas M, Zakar T. Editorial: The Role of the Fetal Membranes in Pregnancy and Birth. Frontiers in Physiology. 2021;12:653084. doi:10.3389/fphys.2021.653084.

5. Preterm birth; 2023. Available from: https://www.who.int/news-room/fact-sheets/detail/preterm-birth.

6. Vink J, Myers K. Cervical alterations in pregnancy. Best Practice & Research Clinical Obstetrics & Gynaecology. 2018;52:88–102. doi:10.1016/j.bpobgyn.2018.03.007.

7. Spontaneous preterm birth: Overview of risk factors and prognosis;. Available from: `https://www.uptodate.com/contents/spontaneous-preterm-birth-overview-of-risk-factors-and-prognosis`.

8. What treatments are used to prevent preterm labor and birth?;. Available from: `https://www.nichd.nih.gov/health/topics/preterm/conditioninfo/treatments`.

9. Commissioner Oot. Modeling & Simulation at FDA. FDA. 2022;.

10. Assessing Credibility of Computational Modeling Through Verification and Validation: Application to Medical Devices; 2018.

11. Galappaththige S, Gray RA, Costa CM, Niederer S, Pathmanathan P. Credibility assessment of patient-specific computational modeling using patient-specific cardiac modeling as an exemplar. PLOS Computational Biology. 2022;18(10):e1010541. doi:10.1371/journal.pcbi.1010541.

12. Wang X, Neu CP, Pierce DM. Advances toward multiscale computational models of cartilage mechanics and mechanobiology. Current Opinion in Biomedical Engineering. 2019;11:51–57. doi:10.1016/j.cobme.2019.09.013.

13. Xu J, Wang Y, Gomez H, Feng X. Biomechanical modelling of tumor growth with chemotherapeutic treatment: a review. Smart Materials and Structures. 2023;32(10):103002. doi:10.1088/1361-665X/acf79a.

14. Debras E, Capmas P, Maudot C, Chavatte-Palmer P. Uterine wound healing after caesarean section: A systematic review. European Journal of Obstetrics and Gynecology and Reproductive Biology. 2024;296:83–90. doi:10.1016/j.ejogrb.2024.02.045.

15. Scott AK, Louwagie EM, Myers KM, Oyen ML. Biomechanical Modeling of Cesarean Section Scars and Scar Defects. bioRxiv. 2023;doi:10.1101/2023.11.03.565565.

16. Gillespie EC. Principles of uterine growth in pregnancy. American Journal of Obstetrics and Gynecology. 1950;59(5):949–959.

17. Sokolowski P, Saison F, Giles W, McGrath S, Smith D, Smith J, et al. Human Uterine Wall Tension Trajectories and the Onset of Parturition;5(6):e11037. doi:10.1371/journal.pone.0011037.

18. Badir S, Mazza E, Zimmermann R, Bajka M. Cervical softening occurs early in pregnancy: Characterization of cervical stiffness in 100 healthy women using the aspiration technique. Prenatal Diagnosis. 2013;doi:10.1002/pd.4116.

19. Du L, Lin MF, Wu LH, Zhang LH, Zheng Q, Gu YJ, et al. Quantitative elastography of cervical stiffness during the three trimesters of pregnancy with a semiautomatic measurement program: A longitudinal prospective pilot study. Journal of Obstetrics and Gynaecology Research. 2020;46(2):237–248. doi:10.1111/jog.14170.

20. Louwagie EM, Carlson L, Over V, Mao L, Fang S, Westervelt A, et al. Longitudinal ultrasonic dimensions and parametric solid models of the gravid uterus and cervix. PLOS ONE. 2021;16(1):e0242118. doi:10.1371/journal.pone.0242118.

21. Carlson LC, Hall TJ, Rosado-Mendez IM, Mao L, Feltovich H. Quantitative assessment of cervical softening during pregnancy with shear wave elasticity imaging: An in vivo longitudinal study. Interface Focus. 2019;9(5). doi:10.1098/rsfs.2019.0030.

22. Kyvernitakis I, Lauer P, Malan M, Badir S, Maul H. A novel aspiration technique to assess cervical remodelling in patients with or without cervical shortening: Sequence of first changes, definition of cut-off values and impact of cervical pessary, stratified for cervical length. PLOS ONE. 2023;18(4):e0283944. doi:10.1371/journal.pone.0283944.

23. Everything you need to know about using the Pregnolia System;. Available from: https://en.pregnolia.com/gebrauchsanweisung.

24. Hadlock FP, Harrist RB, Sharman RS, Deter RL, Park SK. Estimation of fetal weight with the use of head, body, and femur measurements–a prospective study. American Journal of Obstetrics and Gynecology. 1985;151(3):333–337. doi:10.1016/0002-9378(85)90298-4.

25. Schneider CA, Rasband WS, Eliceiri KW. NIH Image to ImageJ: 25 years of image analysis. Nature Methods. 2012;9(7):671–675. doi:10.1038/nmeth.2089.

26. Westervelt AR, Fernandez M, House M, Vink J, Nhan-Chang CL, Wapner R, et al. A Parameterized Ultrasound-Based Finite Element Analysis of the Mechanical Environment of Pregnancy. Journal of Biomechanical Engineering. 2017;139(5):051004. doi:10.1115/1.4036259.

27. R Core Team. R: A Language and Environment for Statistical Computing; 2023. Available from: https://www.R-project.org/.

28. Stone J, House M. Measurement of cervical softness before cerclage placement with an aspiration-based device. American Journal of Obstetrics & Gynecology MFM. 2023;5(4):100881. doi:10.1016/j.ajogmf.2023.100881.

29. Fang S, Shi L, Vink JSY, Feltovich H, Hall TJ, Myers KM. Equilibrium Mechanical Properties of the Nonhuman Primate Cervix;146(8):081001. doi:10.1115/1.4064558.

30. Yoshida K, Jayyosi C, Lee N, Mahendroo M, Myers KM. Mechanics of cervical remodelling: insights from rodent models of pregnancy;9(5):20190026. doi:10.1098/rsfs.2019.0026.

31. Nallasamy S, Palacios HH, Setlem R, Colon Caraballo M, Li K, Cao E, et al. Transcriptome and proteome dynamics of cervical remodeling in the mouse during pregnancy;105(5):1257–1271. doi:10.1093/biolre/ioab144.

32. Yoshida K, Jiang H, Kim M, Vink J, Cremers S, Paik D, et al. Quantitative Evaluation of Collagen Crosslinks and Corresponding Tensile Mechanical Properties in Mouse Cervical Tissue during Normal Pregnancy;9(11):e112391. doi:10.1371/journal.pone.0112391.

33. Degani S, Leibovitz Z, Shapiro I, Gonen R, Ohel G. Myometrial thickness in pregnancy: longitudinal sonographic study.;17(10):661–665. doi:10.7863/jum.1998.17.10.661.

34. Ginsberg Y, Goldstein I, Lowenstein L, Weiner Z. Measurements of the lower uterine segment during gestation;41(4):214–217. doi:10.1002/jcu.22023.

35. Durnwald CP, Mercer BM. Myometrial thickness according to uterine site, gestational age and prior cesarean delivery;21(4):247–250. doi:10.1080/14767050801926709.

36. Hernandez-Andrade E, Hassan SS, Ahn H, Korzeniewski SJ, Yeo L, Chaiworapongsa T, et al. Evaluation of cervical stiffness during pregnancy using semiquantitative ultrasound elastography. Ultrasound in Obstetrics & Gynecology. 2013;41(2):152–161. doi:10.1002/uog.12344.

37. Muller M, Aït-Belkacem D, Hessabi M, Gennisson JL, Grangé G, Goffinet F, et al. Assessment of the Cervix in Pregnant Women Using Shear Wave Elastography: A Feasibility Study. Ultrasound in Medicine & Biology. 2015;41(11):2789–2797. doi:10.1016/j.ultrasmedbio.2015.06.020.

38. Ono T, Katsura D, Yamada K, Hayashi K, Ishiko A, Tsuji S, et al. Use of ultrasound shear-wave elastography to evaluate change in cervical stiffness during pregnancy. Journal of Obstetrics and Gynaecology Research. 2017;43(9):1405–1410. doi:10.1111/jog.13379.

39. Liu Y, Yang D, Jiang Y, Yue Q. Quantification of cervical stiffness changes in single and twin pregnancies using the E-Cervix technique. American Journal of Obstetrics & Gynecology MFM. 2023;5(2):100804. doi:10.1016/j.ajogmf.2022.100804.

40. Rohr Thomsen C, Leonhard AK, Strandbo Schmidt Jensen M, Bor P, Hinge M, Uldbjerg N, et al. Quantitative strain elastography of the uterine cervix assessed by the GE Voluson E10 system in combination with a force-measuring device. The Journal of Maternal-Fetal & Neonatal Medicine. 2023;36(1):2213797. doi:10.1080/14767058.2023.2213797.

41. Papageorghiou AT, Kennedy SH, Salomon LJ, Ohuma EO, Cheikh Ismail L, Barros FC, et al. International standards for early fetal size and pregnancy dating based on ultrasound measurement of crown–rump length in the first trimester of pregnancy;44(6):641–648. doi:10.1002/uog.13448.

42. Kiserud T, Piaggio G, Carroli G, Widmer M, Carvalho J, Jensen LN, et al. The World Health Organization Fetal Growth Charts: A Multinational Longitudinal Study of Ultrasound Biometric Measurements and Estimated Fetal Weight;14(1):e1002220. doi:10.1371/journal.pmed.1002220.

43. Owen J, Albert PS, Buck Louis GM, Fuchs KM, Grobman WA, Kim S, et al. A Contemporary Amniotic Fluid Volume Chart for the United States: The NICHD Fetal Growth Studies-Singletons;221(1):67.e1–67.e12. doi:10.1016/j.ajog.2019.02.030.

44. Berghella V. Contractions of the lower uterine segment during transvaginal ultrasound cervical length: incidence, significance, proper measurement, and management; p. 101303. doi:10.1016/j.ajogmf.2024.101303.
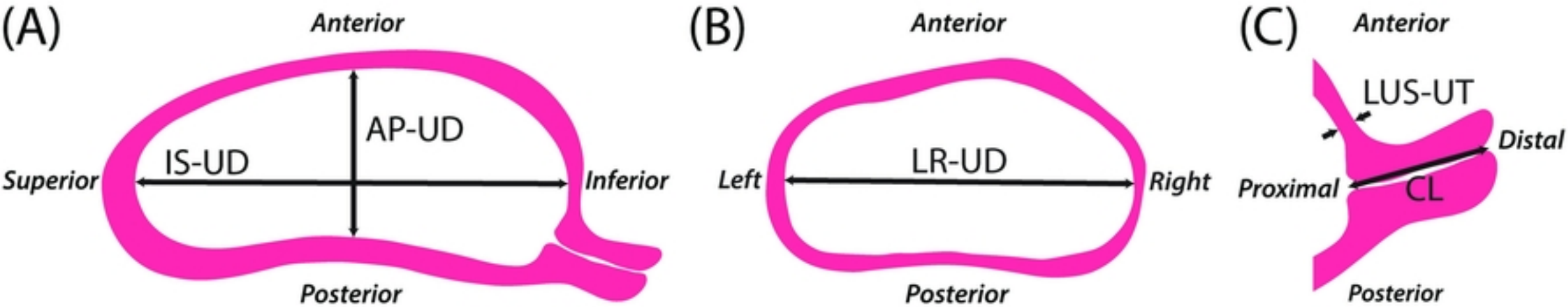
Figure of analyzed measurements
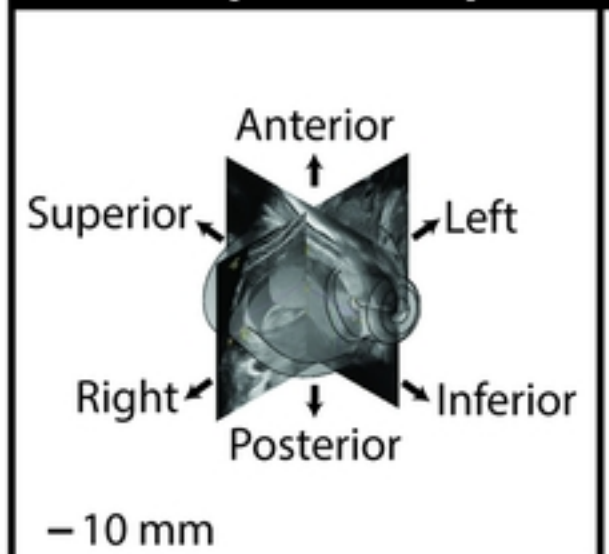
	L1 (12w6d)	M2 (18w6d)	L2 (25w5d)	M3 (35w6d)

Anterior, Superior, Left, Right, Inferior, Posterior

– 10 mm
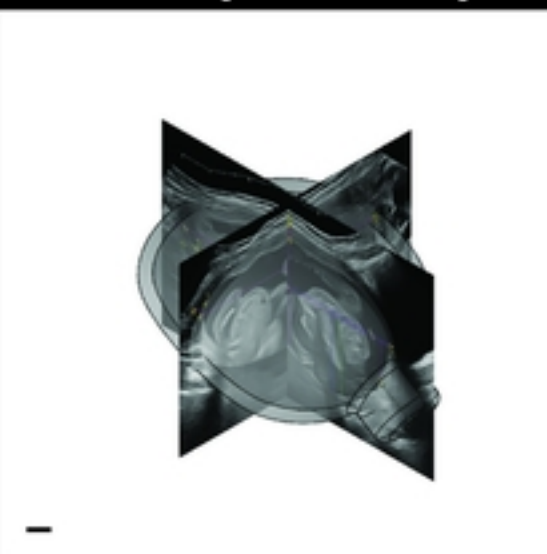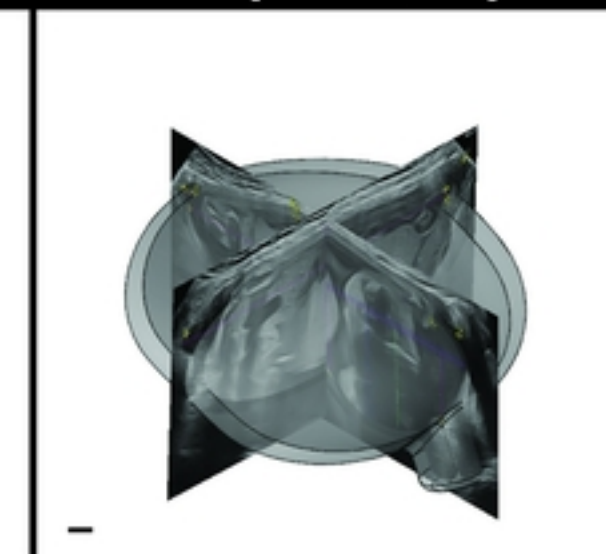
AP-UD, IS-UD
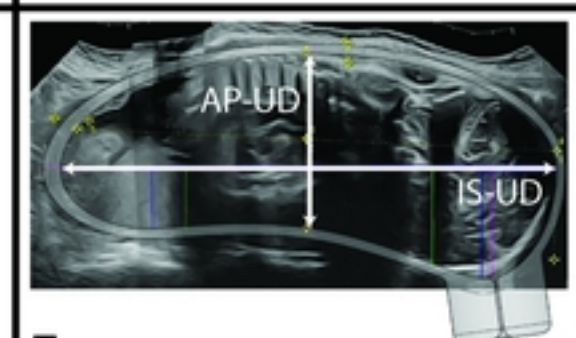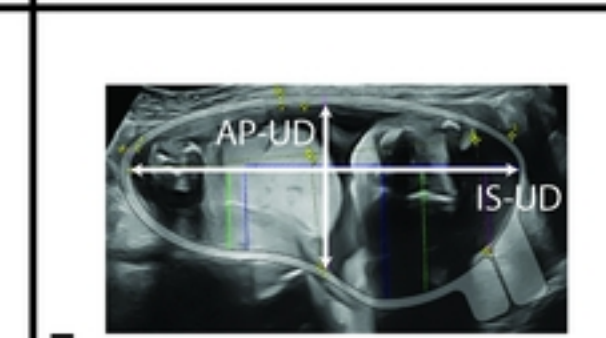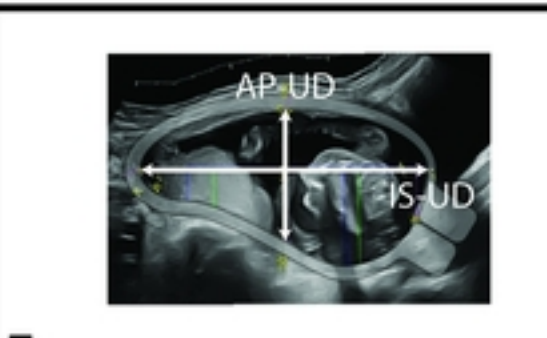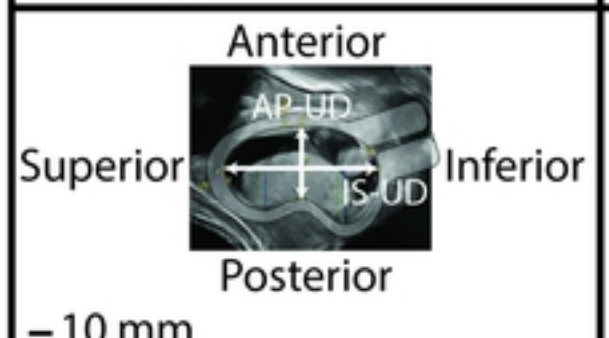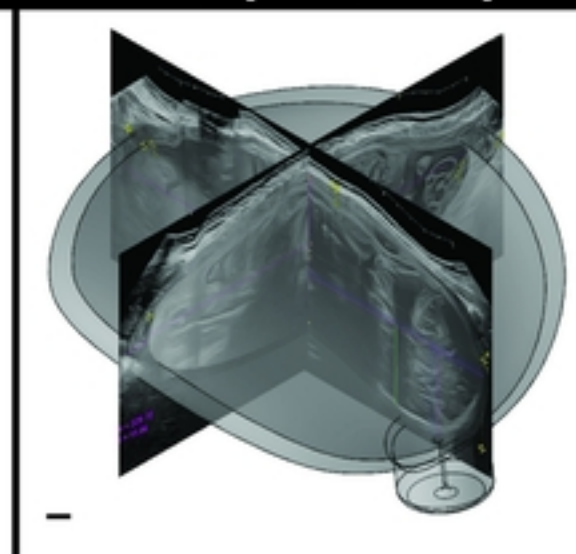
Figure of digital models
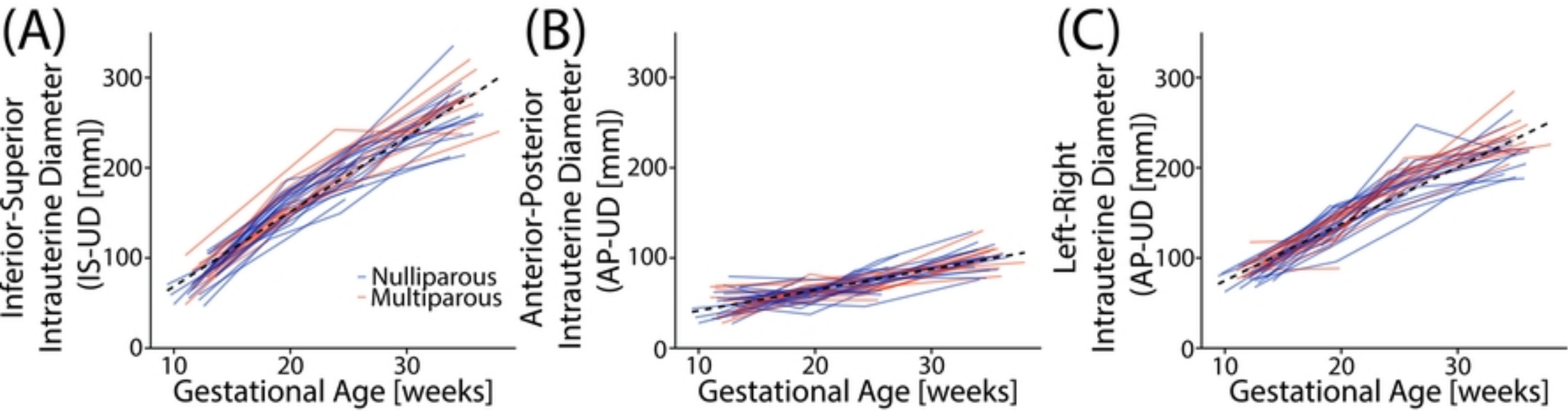
Figure of uterine diameters with gestational age
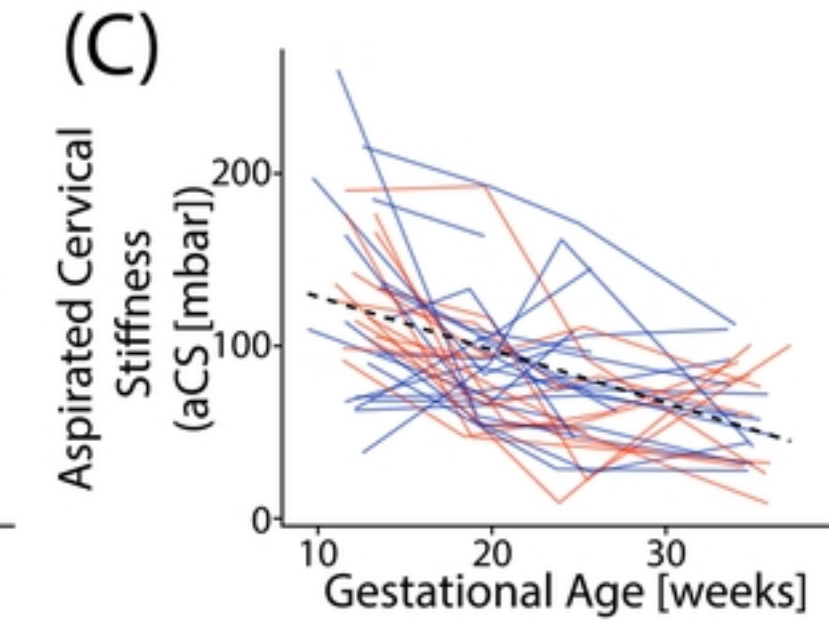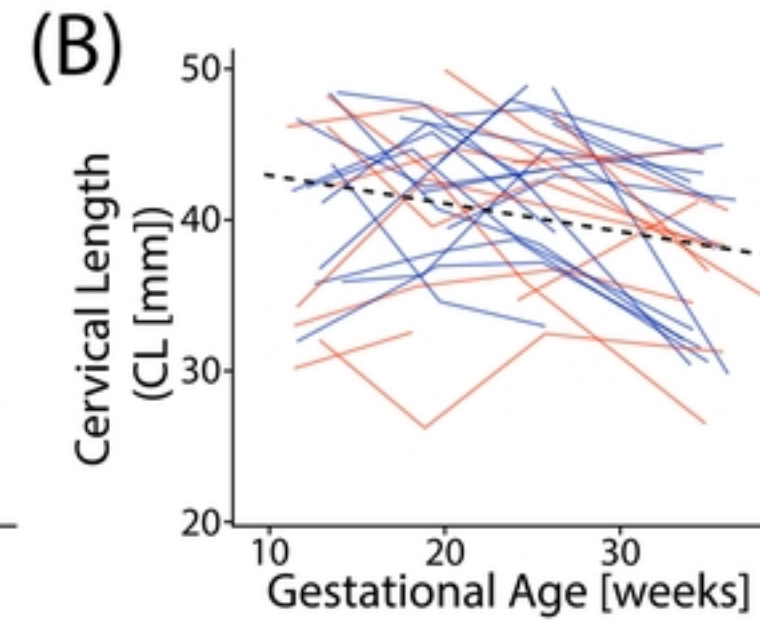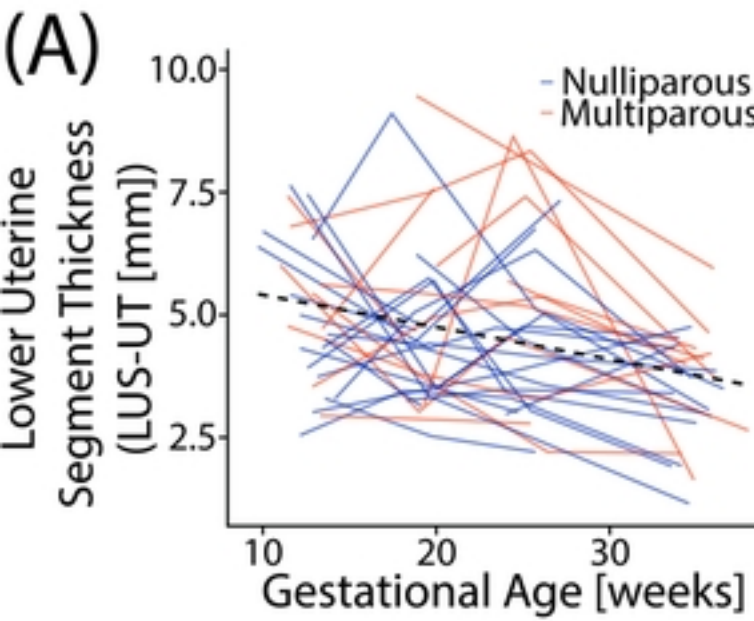
Figure figure of cervical measurements with gestational age
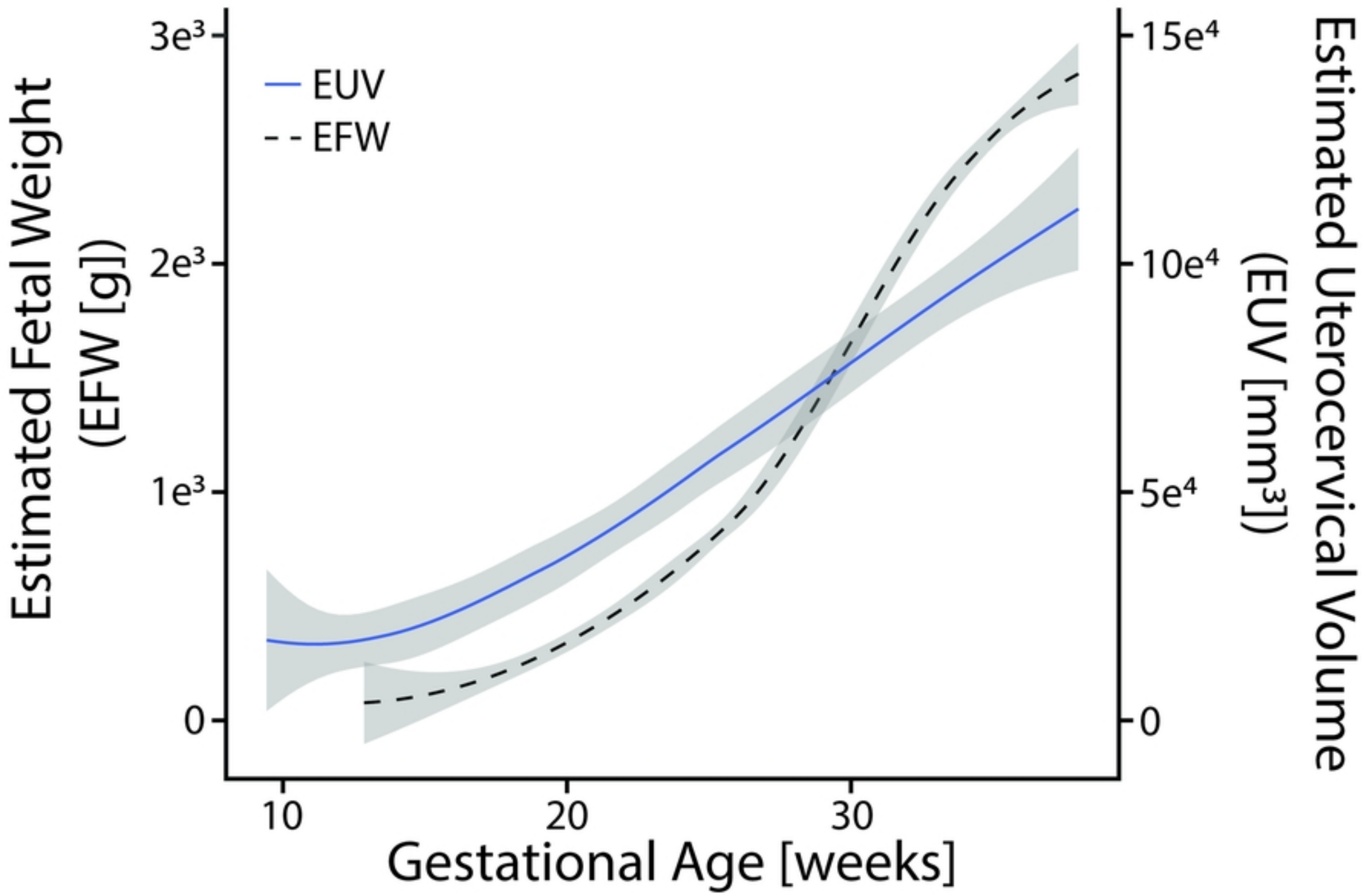
Figure figure of estimated fetal weight and estimated uterocervi
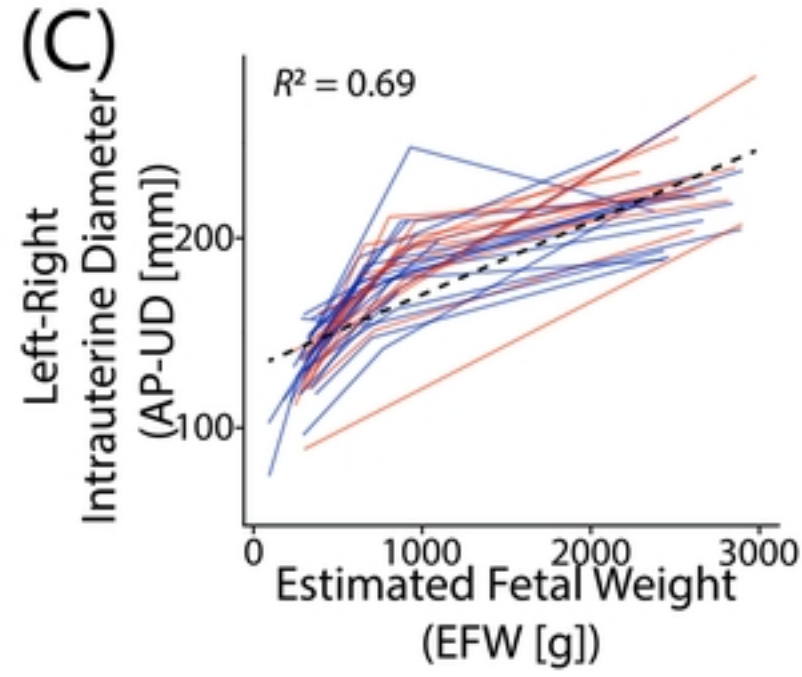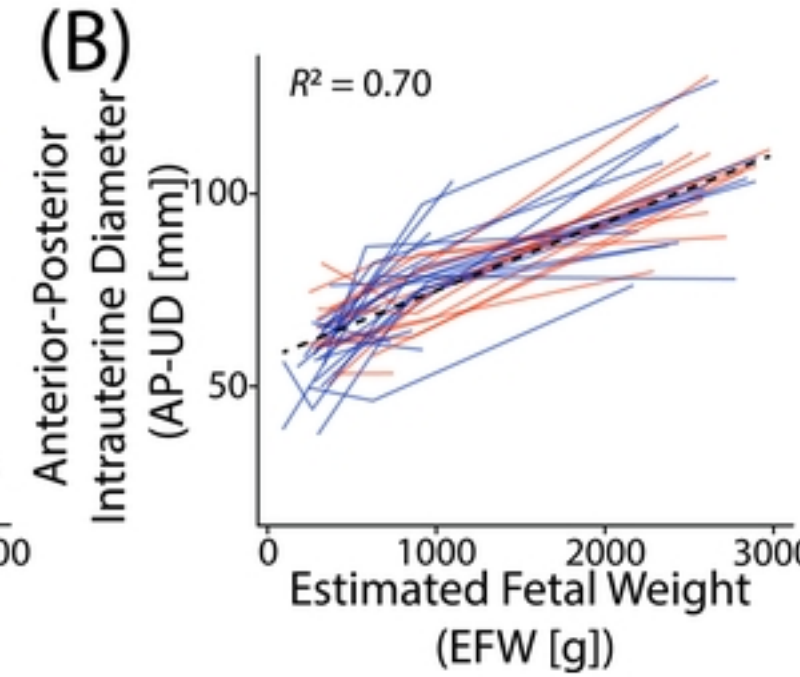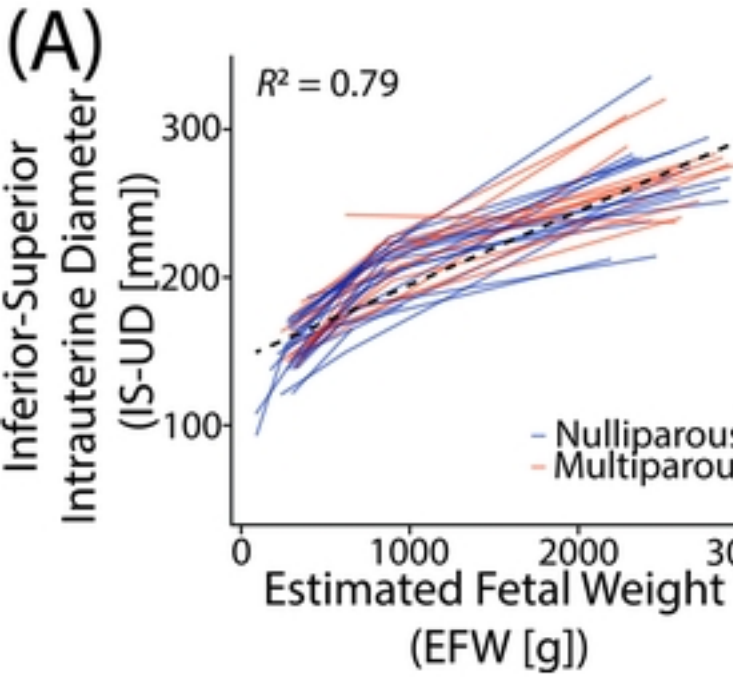
Figure of uterine diameters with estimated fetal weight